# ER reorganization and intracellular retention of CD58 are functionally independent properties of the human cytomegalovirus ER resident glycoprotein UL148

Christopher C. Nguyen,[a] Anthony J. Domma,[a] Hongbo Zhang,[a] and Jeremy P. Kamil[a, #]

Department of Microbiology and Immunology, LSU Health Sciences Center, Shreveport, Louisiana, USA[a]

Running Head: Charged-cluster-to-alanine mutagenesis of HCMV UL148

#Address correspondence to Jeremy P. Kamil, jkamil@lsuhsc.edu

1501 Kings Highway, Shreveport, Louisiana 71103

**ABSTRACT**

The human cytomegalovirus (HCMV) endoplasmic reticulum (ER)-resident glycoprotein UL148 is posited to play roles in immune evasion and regulation of viral cell tropism. UL148 prevents cell surface presentation of the immune cell costimulatory ligand CD58 while promoting maturation and virion incorporation of glycoprotein O, a receptor binding subunit for an envelope glycoprotein complex involved in entry. Meanwhile, UL148 activates the unfolded protein response (UPR) and causes large-scale reorganization of the ER. In an effort to determine whether the seemingly disparate effects of UL148 are related or discrete, we generated charged-cluster-to-alanine (CCTA) mutants of six charged clusters within the UL148 ectodomain, and compared them against wildtype UL148, both in the context of recombinant viruses and in ectopic expression, assaying for effects on ER remodeling and CD58 surface presentation. Two mutants, targeting charged clusters spanning residues 79-83 (CC3) and 133-136 (CC4), respectively, retained the potential to impede CD58 presentation, and did so to an extent comparable to wildtype. Of the six mutants, only CC3 retained the capacity to reorganize the ER, showing a partial phenotype. Wildtype UL148 accumulates in a detergent-insoluble form during infection. However, all six CCTA mutants were fully soluble, which may imply a relationship between insolubility and organelle remodeling. Additionally, we found that the chimpanzee cytomegalovirus UL148 homolog suppresses CD58 presentation but fails to reorganize the ER, while the homolog from rhesus cytomegalovirus shows neither activity. Collectively, our findings illustrate varying functional divergence between homologous primate cytomegalovirus ER immunevasins and suggest that ER reorganization is unique to HCMV UL148.

45 **IMPORTANCE**

46 In myriad examples, viral gene products cause striking effects on cells, such as
47 activation of stress responses. It can be challenging to decipher how such effects
48 contribute to the biological roles of the proteins. The HCMV glycoprotein UL148 retains
49 CD58 within the ER, thereby preventing it from reaching the cell surface where it functions
50 to stimulate cell-mediated antiviral responses. Intriguingly, UL148 also triggers the
51 formation of large, ER-derived membranous structures, and activates the UPR, a set of
52 signaling pathways involved in adaptation to ER stress. We demonstrate that the
53 potential of UL148 to reorganize the ER and to retain CD58 are separable by mutagenesis
54 and possibly, by evolution, since chimpanzee cytomegalovirus UL148 retains CD58 but
55 does not remodel the ER. Our findings imply that ER reorganization contributes to other
56 roles of UL148, such as modulation of alternative viral glycoprotein complexes that govern
57 the virus' ability to infect different cell types.

58

59 **INTRODUCTION**

60 Cytomegaloviruses (CMVs), like other herpesviruses, encode a large and
61 multifarious array of gene products and regulatory RNAs that alter host cell functions to
62 support viral replication, spread, and lifelong persistence [reviewed in (1, 2)]. CMVs have
63 evolved a number of functions that dampen antiviral responses that would otherwise
64 produce sterilizing immunity. Rodent and primate cytomegalovirus (CMV) species, such
65 as mouse cytomegalovirus (MCMV) and human cytomegalovirus (HCMV), express a
66 large number of proteins and microRNAs that interfere with antigen presentation and
67 prevent activation of cytotoxic T cells and NK cells [reviewed in (3-6)], (7). In HCMV,
68 several viral gene products involved in immune evasion, such as UL141 (8, 9), UL142
69 (10-12), and UL148 (13), are encoded within a region of the genome termed the 'UL*b'*,'
70 which undergoes extensive rearrangements and deletions during extensive serial
71 passage in cultured cells (14-16).

72 The HCMV glycoprotein UL148 impedes the activation of cytotoxic T-cell and NK
73 cell mediated responses by binding to the co-stimulatory ligand CD58 and retaining it
74 within the endoplasmic reticulum (ER) (13). UL148 also shows a strong capacity to
75 influence HCMV cell tropism (17, 18). In brief, UL148 appears to stabilize immature forms
76 of glycoprotein O (gO) within the ER, thereby promoting the maturation and incorporation
77 into virions of the heterotrimeric glycoprotein H (gH)/ glycoprotein L (gL)/ gO complex.
78 Since gH/gL/gO is one of the two alternative gH/gL complexes that endow virus with the
79 ability to utilize specific host cell surface receptors during entry, in this case with gO being
80 required to achieve cell entry via PDGFR$\alpha$, which is well expressed in fibroblasts but
81 poorly expressed in epithelial cells (19-22), the effects of UL148 on trimer expression are

82 thought to account for the ~100-fold improved replication of *UL148*-null viruses in
83 epithelial cells (17, 18).

84 Furthermore, UL148 is necessary and sufficient to activate the unfolded protein
85 response (UPR) (23), a canonical ER-stress adaptation pathway conserved among
86 eukaryotes. Although the mechanism for UPR activation remains unknown, UL148
87 appears to interact with the core ER-associated degradation (ERAD) factor SEL1L (18).
88 Hence, UL148 might be hypothesized to cause ER stress by impairing the ability of the
89 SEL1L/Hrd1 complex to dispose of misfolded proteins. Furthermore, UL148 drastically
90 reorganizes the ER, causing the accumulation of unusual electron-dense membranous
91 structures that appear to derive from distended rough-ER cisternae (24). These ER
92 structures are replete with factors involved in glycoprotein quality control such as SEL1L,
93 Hrd1, and EDEM1. We wondered whether the dramatic effects of UL148 on the ER might
94 be related to its potential to retain CD58. We therefore sought to develop experimental
95 approaches to interrogate whether these two UL148-dependent activities were separable
96 or interdependent.

97 In the absence of a three-dimensional structure, charged-cluster-to-alanine
98 (CCTA) mutagenesis provides a useful approach to identify functionally important
99 residues within a protein sequence. The underlying rationale is based on the assumption
100 that charged clusters of amino acids are more likely to be found on solvent exposed
101 surfaces in the context of the tertiary structure of a given polypeptide, and therefore
102 mutations affecting such residues are less likely to strongly influence overall protein
103 folding or stability (25-28). Additionally, charged clusters are often involved in biologically
104 relevant protein-protein interactions, as evidenced by the historical utility of CCTA

105 mutagenesis for identifying residues involved in ligand-receptor interactions (25, 29-32).
106 To define which UL148-associated activities may arise from shared versus distinct
107 molecular mechanisms, we combined CCTA mutagenesis with marker-less bacterial
108 artificial chromosome (BAC) recombination ("recombineering") methods (33, 34) to
109 generate HCMV genomes mutated for individual charged clusters within *UL148*. We also
110 constructed vectors for transient ectopic expression of UL148 CCTA mutants in non-
111 infected cells. Finally, we cloned UL148 homologs from other primate cytomegaloviruses,
112 including chimpanzee CMV (53% amino acid identity with UL148) and rhesus macaque
113 CMV (25% amino acid identity), so as to gain insight into potential evolutionary
114 relationships between the various activities of HCMV UL148.
115
116 **RESULTS**
117
118 **UL148 charged-cluster-to-alanine mutagenesis**
119 In order to identify charged residues within UL148 in an unbiased manner, we
120 utilized a simple scanning algorithm (window = 6 residues) to analyze the predicted
121 ectodomain of UL148. We designated any window containing at least 40% charged
122 amino acids (K, R, D, E) to be a charged cluster (**FIG 1A**). For practical purposes, we
123 opted to treat as a single cluster three clusters that were found in very close proximity to
124 each other (residues 220-231). In this manner, we were able to focus our mutagenesis
125 strategy on six charged clusters within the UL148 ectodomain (**FIG 1B**). We constructed
126 a series of expression plasmids encoding HA-tagged UL148 harboring CCTA mutations
127 at each of the clusters. For comparative purposes, we also cloned UL148 homologs from

128 two other primate CMVs—notably UL148 homologs are found only in primate CMVs. In
129 particular, we constructed plasmids encoding chimpanzee CMV UL148 (Ch148; 53%
130 identity) and rhesus CMV Rh159 (25% identity), each appended at its C-terminus with an
131 HA tag.
132
133 **Expression of UL148 CCTA mutants and UL148 homologs.**
134 As a first step to confirm the expression of the UL148 CCTA mutants, and the
135 primate CMV homologs of UL148, we transfected HEK-293T (293T) cells with each of the
136 different expression plasmids. Robust levels of protein expression were observed for
137 both Rh159 and Ch148 (**FIG 2**). HCMV UL148 expressed to visibly lower levels than
138 Rh159 or Ch148 during a transient overexpression in transfected cells. We interpret the
139 somewhat lower peak expression level of HCMV UL148 as likely being due to its
140 activation of the unfolded protein response (23). Nonetheless, each of the CCTA mutants
141 expressed at levels comparable to that of wildtype UL148, except perhaps CCTA mutant
142 #6, which affected the largest cluster (residues 220-231). Overall, each of the CCTA
143 constructs was readily detected following transient transfection of 293T cells (**FIG 2**).
144
145 **Disruption of four out of six charged clusters abolishes UL148-dependent**
146 **suppression of cell surface CD58**
147 Wang *et al*. (13) reported that HCMV UL148 is necessary and sufficient to
148 suppress surface presentation of CD58, a ligand for CD2 that co-stimulates T and NK cell
149 activation, such as in response to HCMV infection. Since CCTA mutagenesis has been
150 extensively used to define “interface” residues involved in protein-protein interactions, we

151 asked whether UL148 mutants ablated for specific charged clusters would show
152 differences in their ability to suppress CD58 surface presentation. Turning to a transient
153 expression system to ask this question, we electroporated UL148-CCTA constructs into
154 A549 lung adenocarcinoma cells, which basally express surface CD58 (see below). In
155 order to limit our analyses to cells that took up plasmid, we co-transfected a GFP
156 expression vector along with each UL148 construct. Gating for GFP positive cells, we
157 observed a ~40% decrease in CD58 median fluorescence intensity (MFI) in cells
158 transfected with wildtype UL148 (**FIG 3A**). A comparable decrease in surface CD58 was
159 detected in cells transfected with Ch148 expression vector but not with the vector
160 expressing the rhesus CMV UL148 homolog, Rh159. Importantly, four of our six CCTA
161 mutants failed to downregulate surface CD58. The remaining two CCTA constructs,
162 however, mutated at charged clusters #3 (CC3) or #4 (CC4), (**FIG 1B**), suppressed CD58
163 surface presentation comparably to the wildtype UL148.

164 We next sought to analyze the importance of these charged clusters in the context
165 of infection. We employed *en passant* mutagenesis to construct HCMV recombinants
166 harboring these CCTA mutations. Upon infection of fibroblasts with these CCTA mutants,
167 we obtained results that largely recapitulated our findings in nucleofected A549 cells (**FIG**
168 **3B**). The four different charged clusters identified to be required for CD58 suppression in
169 transient transfection likewise were found to be required to suppress CD58 surface
170 presentation in the context of HCMV infection. Moreover, the two CCTA mutants
171 competent for CD58 suppression in transfected A549 cells, CC3 and CC4, likewise
172 appeared to suppress CD58 and did so indistinguishably from parental wildtype virus.
173 These results suggest that the two charged clusters at 79-83 (CC3) and 133-136 (CC4)

174 are dispensable for intracellular retention of CD58. Additionally, our results indicate that
175 the other four charged clusters are either directly required to prevent surface presentation
176 of CD58, or otherwise necessary for UL148 to properly fold or function, since these mutant
177 viruses phenocopy *UL148*-null virus, ($148_{STOP}$), in failing to downregulate CD58 surface
178 levels.
179
180 **The propensity of UL148 to accumulate in a detergent-insoluble form is**
181 **dispensable for suppression of CD58 surface presentation.**
182 We recently observed that UL148 accumulates in a detergent-insoluble form
183 during infection (24). We therefore wished to examine whether any of the CCTA
184 mutations affected the solubility of UL148 during infection, since this could provide a clue
185 as to whether the UL148 insolubility is required for retention of CD58. We carried out
186 these experiments using fibroblasts infected with a series of recombinant HCMVs
187 expressing the six different CCTA mutants, so as to minimize the potential for artifacts
188 concerning solubility that might confound results obtained from transient overexpression
189 of plasmids. Each of the CCTA mutants failed to accumulate in the detergent-insoluble
190 fraction, while wildtype UL148, as expected appeared in both the soluble and insoluble
191 fractions (**FIG 4**). Nonetheless, cells infected with CCTA mutants affecting the clusters #3
192 (residues 79-83) and #4 (residues 133-136) showed defects in CD58 maturation matching
193 those seen with wildtype virus (**FIG 4**), which suggests that the potential for UL148 to
194 accumulate in a detergent-insoluble form is separable from its capacity to prevent CD58
195 maturation.
196

197 **Five out of six charged clusters are necessary for UL148-mediated ER remodeling**

198 UL148 activates the unfolded protein response (UPR), both during infection and
199 ectopic expression (23), and is also necessary and sufficient to drastically remodel the
200 ER (24). Hoping to identify charged clusters necessary for these striking effects, we again
201 turned to our panel of CCTA mutants. Results from confocal immunofluorescence
202 microscopy of infected cells stained for Hrd1 and UL148 (HA tag) at 72 h post-infection
203 (hpi) indicated that five of the six CCTA mutants matched the phenotype seen for *UL148*-
204 null virus ($148_{STOP}$) in failing to cause ER remodeling as indicated by Hrd1 staining (**FIG**
205 **5**). The remaining mutant (CC3) exhibited a partial phenotype wherein UL148 puncta
206 formation could be detected in a minority of cells. Interestingly, the CC4 mutant
207 completely lost the ability to remodel the ER but nonetheless blocks maturation and
208 surface presentation of CD58 similarly if not equivalently to wildtype (**FIG 3-4**). Because
209 both CC3 and CC4 mutants block CD58 surface presentation while exhibiting,
210 respectively, a significant decrease or a complete loss of ER remodeling, these results
211 suggest that these two activities involve distinct molecular mechanisms.

212

213 **The chimpanzee CMV UL148 homolog does not remodel the ER**

214 Lastly, we sought to gain insight into whether the effects of UL148 on the ER and
215 on CD58 surface expression might be conserved by assaying HCMV UL148 against its
216 homologs from other primate CMVs. Rh159, the rhesus CMV homolog, shares 25%
217 amino acid identity with HCMV UL148 and has been shown to retain NKG2D receptor
218 activating ligands of the MIC- and ULBP families (7). Furthermore, Rh159 fails to activate
219 the UPR and does not appear to remodel ER membranes (23, 24). However, the

220 chimpanzee CMV homolog of UL148, Ch148, shares 53% amino acid identity with UL148,
221 and to the best of our knowledge has not been examined for its effects on CD58 or on
222 the ER. We cloned Ch148 fused at its predicted C-terminal tail to eGFP in the context of
223 an inducible expression vector to facilitate observation of Ch148 localization patterns
224 within the cell. We previously constructed similar vectors encoding Rh159 and UL148
225 fused to eGFP (24). Upon induction of protein expression by 100 ng/mL doxycycline, we
226 observed clear formation of puncta for UL148 and diffuse, reticulate signal for Rh159, as
227 previously observed (24). Interestingly, Ch148-eGFP exhibited a diffuse localization
228 pattern more similar to that of Rh159 than UL148 (**FIG 6**). This finding is consistent with
229 the implication from our results with the series of CCTA mutants, that ER remodeling and
230 CD58 retention arise from distinct mechanisms.
231

232 **DISCUSSION**

233

234 **Evidence of distinct mechanisms for CD58 suppression and ER remodeling**

235 Upon discovering that UL148 reorganizes the ER (24), we wondered whether this
236 phenotype might play a role in ER-retention of CD58. We considered the possibility that
237 perhaps CD58 is so efficiently chaperoned to the cell surface that it somehow resists
238 being sequestered via simple high affinity interactions with an ER-resident protein. So
239 perhaps UL148 forms bizarre membranous structures to more potently obstruct its
240 presentation at the cell surface? Two findings from this study argue against this
241 possibility, and instead indicate that ER reorganization is dispensable for UL148-
242 mediated interference with CD58 surface presentation. Firstly, the CCTA mutant affecting
243 charged cluster #4 is fails to remodel the ER but impedes CD58 surface presentation
244 comparably, if not indistinguishably, from wildtype UL148 (**FIG 3-5**). Secondly, the UL148
245 homolog from chimpanzee CMV (Ch148) is sufficient to suppress surface CD58
246 presentation but fails to induce the formation of punctate structures that we consistently
247 observe during expression of HCMV UL148, which indicate ER reorganization (24) (**FIG**
248 **6**). Although we cannot exclude the possibility that Ch148 suppresses CD58 surface
249 presentation by a mechanism distinct from that of HCMV UL148, we consider this to be
250 unlikely, considering the extensive sequence homology between Ch148 and HCMV
251 UL148 (>50% amino acid identity). A summary view of the observed activities for Ch148
252 and UL148 constructs is shown in **FIG 7**. Collectively, the data suggest that the properties
253 of UL148 that give rise to ER re-organization are distinct from those involved in
254 intracellular retention of CD58.

255

256 **Why does UL148 accumulate in a detergent-insoluble form, and what is the**
257 **relationship to ER reorganization?**

258 Fundamental to the biology of the ER is its system of mechanisms, such as N-
259 glycosylation and ER-resident chaperones, that function to prevent proteins from
260 aggregating or accumulating in an insoluble state (35, 36). Therefore, it seems unusual
261 that a wildtype ER resident glycoprotein like UL148 would accumulate in a detergent-
262 insoluble form in the first place. Moreover, this feature of UL148 stands in stark contrast
263 with every other glycoprotein we have analyzed in infected cells, including gB and CD58
264 (**FIG 4**), the RhCMV UL148 homolog Rh159 (24), as well as gH and gO (C.C.N. and
265 J.P.K., unpublished results). Surprisingly, all six of the CCTA mutants examined in this
266 study failed to accumulate in a detergent-insoluble form. Thus, a property readily
267 disrupted by CCTA mutagenesis is required for the protein to accumulate in an insoluble
268 form.

269 Notably, insoluble forms of many different proteins characteristically accumulate
270 during treatments that diminish proteasomal or lysosomal protein degradation pathways
271 (37-39). Moreover, protein aggregates are thought to inhibit the ubiquitin proteasome
272 system (40). Intriguingly, UL148, exhibits a marked tendency toward insolubility even in
273 the absence of such inhibitors. We hypothesize that the native conformer adopted by
274 wildtype UL148 may resist ER associated degradation (ERAD), and perhaps even
275 generally inhibit ERAD. On the other hand, other examples of proteins that form ER
276 structures, such as the Z-allele of alpha-1-antitrypsin (*SERPINA*) (41, 42), or the A103E
277 mutant of the calcium channel subunit ORAI1 (*CRAMC1*), exhibit a propensity to

278 aggregate or polymerize within the ER, which may make them resistant to ERAD. Given
279 their improved solubility, each of the UL148 CCTA mutants, in contrast, might be
280 predicted to be more amenable to ERAD, which may indicate that these mutants no longer
281 aggregate or polymerize, or otherwise lose the ability to inhibit the ERAD machinery.
282 Strikingly, five of the six CCTA mutants fully lost the ability to reorganize the ER,
283 while the one mutant that still showed ER organization exhibited a partial phenotype. It
284 is notable that in all cases, the loss of ER reorganization in the CCTA mutants correlated
285 with markedly improved solubility. These observations collectively suggest that the
286 propensity of UL148 to accumulate in an insoluble form may be mechanistically important
287 for ER remodeling.
288
289 **Roles of ER remodeling cell tropism versus roles in immune evasion?**
290 One might hypothesize ER reorganization to play roles in the cell tropism effects
291 of UL148, given our evidence that it is dispensable for intracellular retention of CD58
292 (**FIGS 3-6**). Our results suggest that ER remodeling is indicative of, if not directly involved,
293 in a function unrelated to CD58 retention. Notably, the effects of UL148 on HCMV cell
294 tropism correlate with its potential to promote the expression of gH/gL/gO, a
295 heterotrimeric complex that endows virions with the ability to utilize PDGFRα as an entry
296 receptor. We previously found that gO behaves as a constitutive ERAD substrate and
297 that UL148 stabilizes its expression. Given that the ER structures induced by UL148
298 contain huge amounts of glycoprotein quality control proteins that participate in ERAD, it
299 seems plausible that UL148 may limit degradation of immature gO by sequestering the
300 ERAD machinery. Therefore, although a role of ER remodeling in suppression of CD58

301 surface presentation seems unlikely, given our findings here, a role in regulation of
302 glycoprotein complexes involved in cell tropism remains to be disproven.
303
304 **Proper folding of UL148 harboring CCTA mutations**
305 In the absence of characterized monoclonal antibodies against UL148, we are
306 limited in our ability to conclusively demonstrate that the UL148 species carrying mutated
307 charged clusters fold properly in the ER. That said, our results offer some insight into the
308 overall stability of the proteins expressed from our plasmid constructs and recombinant
309 viruses. It is notable that all of six of the CCTA mutants we examined in this study show
310 improved solubility relative to wildtype UL148. Insolubility is often associated with
311 misfolding and aggregation. Therefore, the observation that wildtype UL148 is less
312 soluble that its CCTA mutants may suggest that insolubility is important for one or more
313 of its biological functions, but not for CD58 retention, as our results have identified two
314 CCTA mutants that retain CD58 without accumulating in an insoluble form. Even so,
315 caution compels us to avoid making strong conclusions from the other four CCTA mutants
316 that have so far only recapitulated *UL148*-null phenotypes with regard to ER remodeling
317 and CD58 retention. We are therefore focusing on mutants of charged clusters #3 (CC3)
318 and #4 (CC4) in our ongoing studies concerning UL148-mediated ER remodeling, since
319 CCTA mutants of these clusters can be presumed to fold properly, given that they remain
320 able to suppress CD58 maturation.
321
322 **Inferences into the UL148-CD58 interaction face**

323 Alanine scanning and CCTA mutagenesis approaches have proven useful to
324 define the specific amino acid residues underlying biologically relevant protein-protein
325 interactions. Despite that detailed empirical data on the tertiary structure of UL148 as-of-
326 yet remain unavailable, the results from our studies of UL148 CCTA mutants support a
327 number of inferences concerning the physical basis for its interaction with CD58. The two
328 charged clusters that do not appear to be important for CD58 retention, #3 and #4, are
329 found in a contiguous stretch of amino acids (residues 79-136) that lacks other charged
330 clusters. Under the assumption that our other four CCTA mutants do not grossly
331 compromise UL148 folding, residues from the N-terminal half (residues 47-62) and C-
332 terminal half (residues 172-230) of the UL148 ectodomain may, in the ternary structure,
333 participate in an interaction face with CD58. Likewise, we may infer that the contiguous
334 sequence containing clusters #3 and #4 represents a region within the 3D structure that
335 does not participate in CD58 binding.
336
337 **Chimpanzee CMV provides a valuable model for comparative studies of HCMV**
338 **gene products in cell-based assays.**
339 Taken together, our findings highlight the various functionally divergent roles
340 among three different UL148 homologs in CMVs endemic to humans, rhesus
341 macaques, and chimpanzees. While all three of these proteins act as ER resident
342 immunevasins, the rhesus CMV homolog lacks the potential to trigger the UPR (23, 24),
343 and apparently functions to evade NK cells by sequestering MIC- and ULBP family
344 NKG2D ligands from reaching the cell surface (7). Chimpanzee and human CMV
345 UL148 each target CD58 instead of NKG2D ligands, but only HCMV UL148 is capable

346 of remodeling the ER, a property that appears to depend on the capacity to activate the
347 integrated stress response downstream of UPR activation (24). Although chimpanzee
348 CMV is more closely related to HCMV than rhesus CMV, the use of chimpanzees as an
349 animal model for human diseases is prohibited, which likely has limited the interest of
350 researchers in studying the virus. Our study, however, highlights the utility of studying
351 chimpanzee CMV gene products, even in the context of cultured cells, to gain
352 comparative insights into the functions of HCMV genes. Chimpanzee CMV homologs
353 may be of particular importance for helping us to understand the functions of genes in
354 regions of the virus such as the UL*b'*, which are not well conserved, if at all, in rodent
355 CMVs. Moreover, at least in the example of UL148, the chimpanzee homolog appears
356 to be more functionally aligned with HCMV UL148 than the rhesus CMV homolog.
357 Because genes within the UL*b'* play crucial roles in latency, persistence, cell tropism,
358 and immune evasion, elucidating their functions will be of critical importance. A clear
359 picture of which gene specific functions are shared and divergent between the different
360 primate CMVs may provide profound insights into the unique biology of HCMV.

361 **MATERIALS AND METHODS**

362 **Cells.** Human telomerase (hTERT)-immortalized human foreskin fibroblasts (HFFT) were
363 described previously (18), and were cultured in Dulbecco's modified Eagle's medium
364 (DMEM; Corning Cat #10-013-CV) supplemented with 25 µg/mL gentamicin sulfate
365 (Invitrogen), 10 µg/mL ciprofloxacin HCl (Genhunter, Inc.) and 5% newborn calf serum
366 (NCS) (Sigma #N4637). Human embryonic kidney 293T (HEK-293T) cells were obtained
367 from Genhunter, Inc. (Nashville, TN), and cultured in DMEM supplemented as above
368 except with 10% fetal bovine serum (FBS) (MilliporeSigma Cat #F2442) instead of NCS.
369 A549 adenocarcinoma cells were obtained from ATCC (Cat # CCL-185) and grown in
370 Ham's F-12K medium (ThermoFisher, Cat # 21127022) supplemented with 10% FBS and
371 antibiotics, as above.

372

373 **Virus.** Virus was reconstituted by electroporation of purified bacterial artificial
374 chromosome (BAC) DNA into HFFT and amplified until 100% cytopathic effect (CPE) was
375 observed, as previously described (17, 18, 43). Cell-free virus in the medium was
376 combined with cell-associated virus, which was released by Dounce-homogenization of
377 the cells. Virus preparation was clarified of cellular debris by centrifugation (4000 × *g*, 10
378 min), followed by pelleting of virus by ultracentrifugation (85,000 × *g*, 1 h, 4°C) through a
379 20% sorbitol cushion. The supernatant was removed, and the viral pellet was
380 resuspended in DMEM supplemented with 20% NCS and stored at -80°C.

381

382 **Virus titration.** Infectivity of virus stocks was determined according to the tissue culture
383 infectious dose 50% ($TCID_{50}$) method. In brief, stocks were serially diluted, and diluted

384 virus was used to infect eight wells per dilution in a 96-well plate seeded one day prior
385 with 3 × $10^4$ HFFT per well. Infection was allowed to proceed for 9 days before IE1
386 staining as follows. Cells were washed (3 × 200 µL PBS per well) and fixed in ice-cold
387 methanol (200 µL/well, 15 min at -20°C). Cells were washed (3 × 200 µL PBS per well)
388 and stained with 1:200 mouse anti-IE1 primary antibody (supernatant from IE1 mAb 1B12
389 hybridoma cells, a generous gift of Thomas Shenk, Princeton University) for 1 h at 37°C.
390 Cells were washed (3 × 200 µL PBS per well) and stained with 1:1000 goat anti-mouse
391 Alexa Fluor 488 secondary antibody (ThermoFisher, Cat # A-11001) for 1 h at 37°C. The
392 cells were washed (1 × 200 µL PBS per well) and incubated for 1 min with 1 µg/mL
393 Hoechst 33342 (ThermoFisher, Cat# H3570) to counterstain nuclei. Virus plaques were
394 visualized under LED epifluorescence using a Nikon Eclipse Ts2R microscope (Nikon
395 Instruments, Inc, Melville, NY), and each well was scored positive or negative if at least
396 one virus plaque was visible. Infectivity in $TCID_{50}$ units was calculated according to the
397 Spearman-Kärber method, as described previously (18).
398
399 **Plotting of charged clusters within the UL148 ectodomain.** The percentage (charged
400 residues/total residues) in each 6-residue window was plotted using a Python script and
401 visualized using Prism 8 software (GraphPad, Inc., San Diego, CA). Eight local maxima
402 were identified at amino acid positions 47-52, 59-62, 79-83, 133-136, 172-177, 222-225,
403 223-227, 225-230. Because of their close proximity to each other, the final three clusters
404 were regarded as a single charged cluster for the purposes of constructing mutants.
405

406 **Expression vectors encoding HA-tagged UL148 harboring charged-cluster-to-**
407 **alanine mutations.** pcDNA3.1+ UL148HA was generated as follows. A PCR product
408 encoding the HA-tagged *UL148* open reading frame was amplified from template plasmid
409 pEF1α UL148HA (18) using primers UL148_reclone_FWD and UL148_reclone_REV.
410 PCR product was digested with BamHI/EcoRI and ligated into BamHI/EcoRI-digested
411 pcDNA3.1+ (Invitrogen) to yield pcDNA3.1+ UL148HA, which was sequence-confirmed
412 using primers CMV_FWD and BGH_REV.
413 HA-tagged UL148 was subcloned from pcDNA3.1+ into pSP72 as follows.
414 pcDNA3.1+ UL148HA was digested with BamHI/EcoRI. The ~1kb fragment was agarose-
415 purified and ligated into BamHI/EcoRI-digested pSP72. Overlapping primers (Table 1)
416 were used to amplify the pSP72 UL148HA template and introduce charged-cluster-to-
417 alanine (CCTA) mutations into the *UL148* open reading frame (ORF). PCR products were
418 digested with DpnI for 1 h at 37°C to remove template plasmid before transformation and
419 isolation of carbenicillin-resistant clones, which were confirmed by enzyme digestion and
420 sequencing using primers SP6_FWD and T7_seq_FWD. These mutated *UL148*
421 sequences were then transferred back to pcDNA3.1+ by BamHI/EcoRI digestion and
422 ligation as above.
423
424 **Expression vectors encoding HA-tagged chimpanzee CMV UL148 and rhesus CMV**
425 **Rh159.** pcDNA3.1+ Rh159HA was described previously (23). pcDNA3.1+ encoding HA-
426 tagged chimpanzee CMV UL148 was constructed by Gibson assembly of gBlock
427 ChCMV_UL148_FRAG with BamHI/EcoRI-digested pcDNA3.1+ (Invitrogen) and
428 sequence-confirmed using primers CMV_FWD and BGH_REV. The coding sequence

429 for chimpanzee CMV UL148 (Panine herpesvirus 2 strain Heberling, Genbank/ NCBI
430 Reference Sequence: NC_003521.1) was codon-optimized by Integrated DNA
431 Technologies (Coralville, IA), based on *Homo sapiens* codon usage, to facilitate synthesis
432 as a synthetic dsDNA gBlock.
433
434 **Inducible expression vectors encoding EGFP fused to UL148 homologs of human,**
435 **chimpanzee, and rhesus CMV.** Inducible lentiviral vectors pOUPc-UL148-eGFP and
436 pOUPc-Rh159-eGFP were described previously (24). pOUPc encoding chimpanzee
437 CMV UL148 fused to eGFP was constructed as follows. Fragment (i) was amplified using
438 primers Fwd_Ch148_OUPgibs and Rev_Ch148_GFPgibs with pcDNA3.1+ ChCMV
439 UL148HA as a template. Fragment (ii) was amplified using primers Fwd_GFP_Ch148gibs
440 and Rev_GFP_allUL148 using pOUPc-UL148-eGFP as a template. Fragments (i) and (ii)
441 were combined with AgeI/MluI-digested pOUPc in Gibson assembly to yield pOUPc-
442 Ch148-eGFP, which was sequence-confirmed using primers CMVcrsnull_Fw, Ubc_Rv,
443 and Ch148_3pr_Fw.
444
445 **Construction of recombinant viruses.** Synthetic double-stranded DNA (gBlocks) and
446 oligonucleotides were purchased from Integrated DNA Technologies; sequences are
447 provided in **Table 1**. All mutagenesis procedures was performed in the context of the
448 infectious BAC clone of HCMV strain TB40/E, TB40-BAC4 (44), as previously described
449 (17, 18, 23, 43, 45). Briefly, two-step Red "*en passant*" recombination (33, 34) was used
450 in conjunction with GS1783 *E. coli* (a gift of Greg Smith, Northwestern University)
451 harboring derivatives of TB40-BAC4. Recombinant BACs were confirmed by Sanger-

452 sequencing (Genewiz, Inc., South Plainfield, NJ) of modified loci (not shown), and by
453 BamHI and EcoRI restriction enzyme digestion analysis to exclude spurious
454 rearrangements (not shown).
455
456 **Recombinant HCMVs encoding HA-tagged UL148 and S-tagged glycoprotein O.**
457 Recombinant HCMV, strain TB40/E, encoding S-tagged glycoprotein O and HA-tagged
458 UL148 (TB_148$^{HA}$_gO$^{S}$) was constructed by insertion of a S-tag at the C-terminus of the
459 *UL74* open reading frame, essentially as in (18), but in the context of recombinant
460 TB_148$^{HA}$ (17). Briefly, plasmid pSP72-*UL74-S-ISceKan* (18) was digested with EcoRV,
461 and the 1.4 kb band was agarose-purified and recombined into TB_148$^{HA}$. Kan-resistant
462 integrate colonies were isolated and resolved of the Kan cassette by L(+)-arabinose
463 induction of the homing endonuclease ISce-I and the bacteriophage lambda Red
464 recombinase system. Kan-sensitive clones were sequence-confirmed using primers
465 TB_UL74_Cterm_seq_FWD and TB_UL74_Cterm_seq_REV.
466
467 **Recombinant HCMVs encoding CCTA mutations within *UL148*.** CCTA mutations
468 were introduced into TB_148$^{HA}$_gO$^{S}$ as follows. A PCR product containing an I-SceI
469 restriction site upstream of a kanamycin (Kan) resistance cassette and 40-bp flanks
470 homologous to the sequence surrounding each *UL148* charged cluster was amplified
471 using primers indicated in Table 1 and TB_148_ISceKan BAC DNA (17) as the template.
472 The gel-purified PCR product was electroporated into GS1783 *E. coli* carrying an
473 infectious BAC clone of TB_148$^{HA}$_gO$^{S}$. After isolating Kan-resistant colonies, the Kan
474 expression cassette was “scarlessly” resolved by inducing expression of the I-SceI

475 homing endonuclease and Red recombinase. The final Kan-sensitive
476 TB_148$^{HA}$_CCTA_gO$^{S}$ recombinants were sequence-confirmed using primers
477 TB_Rh159HA_seq_FWD and TB_Rh159HA_seq_REV.
478
479 **Antibodies.** Antibody dilutions for Western blot included 1:1000 rabbit anti-HA (Bethyl),
480 1:250 mouse anti-CD58 (Invitrogen #MA5800). For flow cytometry, APC-conjugated
481 mouse anti-CD58 antibody (Invitrogen #17-0578) and isotype control (Invitrogen #17-
482 4714) were used at 1:40 dilution. For confocal microscopy, chicken anti-HA (Bethyl) and
483 rabbit anti-Hrd1 (Cell Signaling Technology) were used at a dilution of 1:200. Goat anti-
484 chicken Alexa Fluor 647 (Invitrogen) and goat anti-rabbit Alexa Fluor 488 (Invitrogen)
485 secondary antibodies were used at 1:1000.
486
487 **Surface CD58 quantification by flow cytometry.** For experiments in transfected cells,
488 $1.2 \times 10^6$ A549 cells were nucleofected using a Lonza Nucleofector™ 2B device
489 (program X-001) with 1.5 µg pcDNA3.1+ encoding the indicated protein plus 1 µg
490 pmaxGFP™ (Amaxa) in Ingenio nucleofection buffer (Mirus, Inc., cat # MIR 50114) .
491 Nucleofected cells were then seeded to a 6-well cluster dish and incubated at 37°C until
492 72 h post-transfection. For experiments in infected fibroblasts, $1.0 \times 10^5$ cells were
493 seeded into 6-well cluster dishes and infected at an MOI of 2 $TCID_{50}$/cell with
494 TB_148$_{HA}$_gO$^{S}$ or the derived CCTA mutant viruses. The following day, the viral inocula
495 were removed, and media were replenished with fresh 5% newborn calf serum
496 (NCS)/DMEM. The cells were incubated at 37˚C until 72 h post-infection. Infected cells
497 were formalin-fixed before the CD58-staining step below.

498 At time of analysis, cells were detached using a 1:10 dilution of TrypLE$^{TM}$
499 Express (Gibco #12605) solution. Cells were pelleted (5 min, 300 × *g*) and resuspended
500 in FACS buffer [5% NCS in PBS]. Cells were incubated with APC-conjugated anti-CD58
501 antibody or isotype control for 1 h at 4°C with rotation, then washed three times with
502 FACS buffer and analyzed by flow cytometry. In transfection experiments, cells were
503 first gated on GFP to remove any non-transfected cells from the analysis. Median APC
504 fluorescence values were determined for each condition, and all values were
505 normalized to the median APC signal of GFP+ cells transfected with empty pcDNA3.1+.
506 Graphs were generated in Prism 8 for Mac Os (GraphPad Software, Inc. San Diego,
507 CA).

508 **Analysis of protein solubility.** 2 × $10^5$ fibroblasts (HFFT) were infected at an MOI of 1
509 $TCID_{50}$ per cell with TB_148$^{HA}$_gO$^{S}$ or the derived CCTA mutants. The following day,
510 cells were washed once with PBS and replenished with fresh 5% NCS/DMEM. At 72 h
511 post-infection, cells were prepared for Western blot analysis of detergent-soluble and -
512 insoluble material as previously described (24). Briefly, cells were washed with PBS and
513 lysed by direct addition of RIPA buffer [25 mM 4-(2-hydroxyethyl)-1-
514 piperazineethanesulfonic acid (HEPES) pH 7.5, 400 mM NaCl, 0.1% sodium dodecyl
515 sulfate (SDS), 0.5% sodium deoxycholate, 1% NP-40], supplemented with 1× protease
516 inhibitor cocktail (ApexBio, Inc., Houston, TX, Cat #K1007) and rotated for 1 h at 4˚C.
517 Lysates were centrifuged (21,000 × *g*, 35 min) to separate soluble and insoluble
518 material. The supernatant containing soluble material was transferred to a new tube,
519 and Laemmli buffer was added to 1× final [50 mM Tris (pH 6.8), 2% SDS, 10% glycerol,
520 0.02% bromophenol blue]. Pellet containing insoluble material was lysed in 1× Laemmli

521 buffer. Samples were reduced by addition of beta-mercaptoethanol (5% final, v/v) and
522 boiled at 90˚C for 10 min. Samples were resolved by SDS-PAGE (12% polyacrylamide
523 gel) and transferred to nitrocellulose membrane. Membranes were blotted with indicated
524 antibodies and visualized by Odysey CLx scanner (Li-Cor, Inc., Lincoln, NE).

525

526 **Plasmid transfection.** For Western blot studies, 1 × $10^6$ HEK-293T (293T) cells were
527 reverse-transfected with 2.5 µg pcDNA3.1+ encoding the indicated proteins, as follows.
528 TransIT-293 transfection reagent (Mirus Inc., Madison, WI, Cat #2700) was mixed with
529 plasmid DNA in Opti-MEM (ThermoFisher) according to the manufacturer's instructions.
530 After 25 min incubation at room temperature, the transfection reagent-DNA complexes
531 were added to 2 mL 5% FBS/DMEM containing 1 × $10^6$ HEK-293T cells in suspension.
532 Cells and transfection reagent-DNA complexes were gently mixed and seeded to a 6-
533 well plate.

534 For immunofluorescence imaging, 7 × $10^4$ 293T cells were reverse-transfected
535 with 1 µg doxycycline-inducible pOUPc plasmid (23, 24) encoding the indicated protein
536 as follows. Plasmid DNA was combined with 7.5 µL of 1 mg/mL branched
537 polyethylenimine (PEI; Sigma #408727) in 160 µL of Opti-MEM and gently mixed. DNA-
538 PEI complexes were allowed to form at room temperature for 20 min. 1 mL of 5%
539 FBS/DMEM containing 7 × $10^4$ 293T cells was then added to the DNA-PEI solution and
540 mixed gently before seeding to a 96-well plate. After cells had attached to the well (1 h
541 post-transfection), doxycycline hyclate stock was added directly to each well to a final

542 concentration of 100 ng/mL. Cells were incubated at 37°C for 48 h before imaging for
543 GFP signal on a Nikon Eclipse Ts2R microscope (Nikon Instruments, Inc, Melville, NY).

544 **Confocal microscopy.** 7 × $10^5$ fibroblasts (HFFT) were seeded on 12 mm round
545 coverslips (Azer Scientific, #200121) in a 24-well plate. The following day, cells were
546 infected at an MOI of 1 $TCID_{50}$ per cell with TB_148$^{HA}$_gO$^{S}$ or the indicated
547 recombinants. At 72 h post-infection, cells were processed for confocal microscopy
548 essentially as in (24). Briefly, cells were washed once with 1 mL PBS, fixed in 4% (w/v)
549 paraformaldehyde/PBS for 20 min at room temperature, and permeabilized for 3 min by
550 0.1% TritonX-100. Coverslips were incubated in 5% (v/v) normal goat serum for 30 min
551 at room temperature. After washing three times with 1 mL PBS, coverslips were
552 incubated with 1% Human Fc Block (BD Biosciences, Cat # 564219) for 30 min at room
553 temperature. Coverslips were incubated with primary antibody for 1 h in a humid 37°C
554 incubator, washed three times in 1 mL PBS and then incubated in the presence of
555 secondary antibody (1 h, 37°C humid incubator), followed by three washes in PBS, as
556 above. Finally, coverslips were mounted onto glass slides in mounting medium [0.01 M
557 Tris (pH 8.8), 90% glycerol, 0.5% N-propyl gallate] and sealed with nail polish. Cells
558 were imaged on a Leica TCS SP5 confocal microscope using a Leica 63× oil immersion
559 objective lens.

560 **ACKNOWLEDGMENTS**

561 This project was supported by NIH Grants R01-AI116851 (to J.P.K) and P30-
562 GM110703. Its contents are solely the responsibility of the authors and do not
563 necessarily represent the official views of the funding agencies. C.C.N. was supported
564 by a Malcolm Feist Predoctoral Fellowship from the Center of Cardiovascular Diseases

565 and Sciences at LSU Health Sciences Center, Shreveport. Author contributions are as
566 follows: C.C.N. conceived of the study, designed research, constructed new
567 recombinant HCMVs and plasmid constructs, carried out most experiments, and
568 contributed to writing the manuscript. A.J.D. performed and contributed to the design of
569 the flow cytometry experiments with infected cells. J.P.K. designed research,
570 interpreted data, obtained funding, and contributed to writing the manuscript. H.Z.
571 assisted with confocal microscopy and constructed the recombinant virus
572 TB_148$^{HA}$_gO$^{S}$.

573 **FIGURE 1. Charged amino acid clusters within the predicted UL148 ectodomain**.
574 (A) Percentage of charged residues (K, R, D, E) within the predicted UL148 ectodomain
575 identified using an iterative scanning window six amino acid residues in size. Black arrows
576 designate charged clusters (>40% charged residues). The last three local maxima in
577 close proximity were treated as a single cluster. (B) UL148 protein sequence. Amino acid
578 positions (pos) of the identified charged clusters are underlined. Residues in red were
579 mutated to alanine in the six constructs indicated above using sequential numbering (ID),
580 starting from the amino-terminus.
581
582 **FIGURE 2. Expression of HA-tagged UL148-CCTAs and UL148 homologs.** Human
583 embryonic kidney 293T cells were transfected with expression plasmids encoding the
584 indicated HA-tagged proteins. At 48 h post-transfection, cell lysates were analyzed by
585 Western blot.
586
587 **FIGURE 3. Analysis of cell surface CD58 levels during expression of UL148 CCTA**
588 **mutants and homologs from other primate CMVs.** (A) A549 cells were transfected
589 with plasmids expressing the indicated protein or empty vector (EV). At 72 h post-
590 transfection, cell surface CD58 levels were analyzed by flow cytometry. Median
591 fluorescence intensity (MFI) values were normalized to the EV control. (B) Fibroblasts
592 (HFFT) were infected at an MOI of 2 $TCID_{50}$ per cell with HCMV strain TB40/E
593 derivatives wildtype for *UL148* (WT), carrying the indicated UL148 CCTA mutations, or
594 *UL148*-null ($148_{STOP}$). At 72 h post-infection, cell surface CD58 was quantified by flow
595 cytometry. (A-B) Data points indicate biological replicates from three independent

596 experiments. P-values comparing the mean of each condition to wildtype UL148
597 (UL148, panel A) or wildtype virus (WT, panel B) were obtained by one-way analysis of
598 variance (ANOVA) with Tukey's correction for multiple comparisons: ns, not significant;
599 *, $p < 0.05$; **, $p < 0.01$; ****, $p < 0.0001$.

600

601 **FIGURE 4. The propensity of UL148 to accumulate in a detergent-insoluble form**
602 **is not required to block CD58 maturation.** Fibroblasts (HFFT) were infected at an
603 MOI of 1 $TCID_{50}$ per cell with HCMV or the indicated *UL148* mutant. At 72 h post-
604 infection, cell lysates were separated by centrifugation into supernatant ("S") containing
605 soluble proteins and pellet ("P") containing insoluble proteins. Supernatant and pellet
606 fractions were analyzed by Western blot for UL148, CD58, and gB levels.

607

608 **FIGURE 5. Mutation of five UL148 charged clusters abolishes punctate co-**
609 **localization of UL148 and ER marker Hrd1.** Fibroblasts (HFFT) were infected at an MOI
610 of 1 $TCID_{50}$ per cell with HCMV strain TB40/E wildtype for *UL148*, harboring the indicated
611 *UL148* CCTA mutant, or entirely null for *UL148* ($148_{STOP}$). At 72 h post-infection, cells
612 were fixed and imaged by confocal microscopy after staining with antibodies specific for
613 HA ($UL148^{HA}$, magenta) or ER marker Hrd1 (green). Nuclei were counterstained using
614 Hoechst dye (blue). Scale bars; left panels: 100 μm, right panels; 25 μm.

615

616 **FIGURE 6. Localization of UL148, Rh159, and Ch148.** Human embryonic kidney 293T
617 cells were transfected with doxycline-inducible vectors encoding the indicated protein

618 fused to a GFP tag. 100 ng/mL doxycycline was added to cells 1 h post-transfection. At
619 48 h post-transfection, GFP signal was visualized by immunofluorescence microscopy.
620
621 **FIGURE 7. Summary of activities of UL148-CCTAs and UL148 homologs.** Green
622 squares indicate activity indistinguishable from wild-type HCMV UL148. Red squares
623 indicate total absence of the activity. Yellow squares indicate a partial phenotype. Gray
624 square, not tested.
625

626 **REFERENCES**


627 1. Jackson SE, Mason GM, Wills MR. 2011. Human cytomegalovirus immunity and
628 immune evasion. Virus Res 157:151-60.
629 2. Mocarski ES, Shenk T, Griffiths PD, Pass RF. 2013. Cytomegaloviruses, p 1960-2014.
630 *In* Knipe DM, Howley PM (ed), Fields' Virology, 6th ed, vol 2. Wolters Kluwer
631 Health/Lippincott Williams & Wilkins, Philadelphia.
632 3. Goodier MR, Jonjic S, Riley EM, Juranic Lisnic V. 2018. CMV and natural killer cells:
633 shaping the response to vaccination. Eur J Immunol 48:50-65.
634 4. Lemmermann NA, Bohm V, Holtappels R, Reddehase MJ. 2011. In vivo impact of
635 cytomegalovirus evasion of CD8 T-cell immunity: facts and thoughts based on
636 murine models. Virus Res 157:161-74.
637 5. Wilkinson GW, Tomasec P, Stanton RJ, Armstrong M, Prod'homme V, Aicheler R,
638 McSharry BP, Rickards CR, Cochrane D, Llewellyn-Lacey S, Wang EC, Griffin CA,
639 Davison AJ. 2008. Modulation of natural killer cells by human cytomegalovirus. J Clin
640 Virol 41:206-12.
641 6. Goldberger T, Mandelboim O. 2014. The use of microRNA by human viruses: lessons
642 from NK cells and HCMV infection. Semin Immunopathol 36:659-74.
643 7. Sturgill ER, Malouli D, Hansen SG, Burwitz BJ, Seo S, Schneider CL, Womack JL,
644 Verweij MC, Ventura AB, Bhusari A, Jeffries KM, Legasse AW, Axthelm MK, Hudson
645 AW, Sacha JB, Picker LJ, Fruh K. 2016. Natural Killer Cell Evasion Is Essential for
646 Infection by Rhesus Cytomegalovirus. PLoS Pathog 12:e1005868.
647 8. Prod'homme V, Sugrue DM, Stanton RJ, Nomoto A, Davies J, Rickards CR, Cochrane
648 D, Moore M, Wilkinson GW, Tomasec P. 2010. Human cytomegalovirus UL141
649 promotes efficient downregulation of the natural killer cell activating ligand CD112.
650 J Gen Virol 91:2034-9.
651 9. Smith W, Tomasec P, Aicheler R, Loewendorf A, Nemcovicova I, Wang EC, Stanton RJ,
652 Macauley M, Norris P, Willen L, Ruckova E, Nomoto A, Schneider P, Hahn G, Zajonc
653 DM, Ware CF, Wilkinson GW, Benedict CA. 2013. Human cytomegalovirus
654 glycoprotein UL141 targets the TRAIL death receptors to thwart host innate
655 antiviral defenses. Cell Host Microbe 13:324-35.
656 10. Ashiru O, Bennett NJ, Boyle LH, Thomas M, Trowsdale J, Wills MR. 2009. NKG2D
657 ligand MICA is retained in the cis-Golgi apparatus by human cytomegalovirus
658 protein UL142. J Virol 83:12345-54.
659 11. Bennett NJ, Ashiru O, Morgan FJ, Pang Y, Okecha G, Eagle RA, Trowsdale J, Sissons JG,
660 Wills MR. 2010. Intracellular sequestration of the NKG2D ligand ULBP3 by human
661 cytomegalovirus. J Immunol 185:1093-102.
662 12. Wills MR, Ashiru O, Reeves MB, Okecha G, Trowsdale J, Tomasec P, Wilkinson GW,
663 Sinclair J, Sissons JG. 2005. Human cytomegalovirus encodes an MHC class I-like
664 molecule (UL142) that functions to inhibit NK cell lysis. J Immunol 175:7457-65.
665 13. Wang ECY, Pjechova M, Nightingale K, Vlahava VM, Patel M, Ruckova E, Forbes SK,
666 Nobre L, Antrobus R, Roberts D, Fielding CA, Seirafian S, Davies J, Murrell I, Lau B,
667 Wilkie GS, Suarez NM, Stanton RJ, Vojtesek B, Davison A, Lehner PJ, Weekes MP,
668 Wilkinson GWG, Tomasec P. 2018. Suppression of costimulation by human
669 cytomegalovirus promotes evasion of cellular immune defenses. Proc Natl Acad Sci
670 U S A 115:4998-5003.

671 14. Cha TA, Tom E, Kemble GW, Duke GM, Mocarski ES, Spaete RR. 1996. Human
672 cytomegalovirus clinical isolates carry at least 19 genes not found in laboratory
673 strains. J Virol 70:78-83.
674 15. Dargan DJ, Douglas E, Cunningham C, Jamieson F, Stanton RJ, Baluchova K, McSharry
675 BP, Tomasec P, Emery VC, Percivalle E, Sarasini A, Gerna G, Wilkinson GW, Davison
676 AJ. 2010. Sequential mutations associated with adaptation of human
677 cytomegalovirus to growth in cell culture. J Gen Virol 91:1535-46.
678 16. Murrell I, Wilkie GS, Davison AJ, Statkute E, Fielding CA, Tomasec P, Wilkinson GW,
679 Stanton RJ. 2016. Genetic Stability of Bacterial Artificial Chromosome-Derived
680 Human Cytomegalovirus during Culture In Vitro. J Virol 90:3929-43.
681 17. Li G, Nguyen CC, Ryckman BJ, Britt WJ, Kamil JP. 2015. A viral regulator of
682 glycoprotein complexes contributes to human cytomegalovirus cell tropism. Proc
683 Natl Acad Sci U S A 112:4471-6.
684 18. Nguyen CC, Siddiquey MNA, Zhang H, Li G, Kamil JP. 2018. Human Cytomegalovirus
685 Tropism Modulator UL148 Interacts with SEL1L, a Cellular Factor That Governs
686 Endoplasmic Reticulum-Associated Degradation of the Viral Envelope Glycoprotein
687 gO. J Virol 92:e00688-18.
688 19. Wu K, Oberstein A, Wang W, Shenk T. 2018. Role of PDGF receptor-alpha during
689 human cytomegalovirus entry into fibroblasts. Proc Natl Acad Sci U S A
690 doi:10.1073/pnas.1806305115.
691 20. Wu Y, Prager A, Boos S, Resch M, Brizic I, Mach M, Wildner S, Scrivano L, Adler B.
692 2017. Human cytomegalovirus glycoprotein complex gH/gL/gO uses PDGFR-alpha
693 as a key for entry. PLoS Pathog 13:e1006281.
694 21. Vanarsdall AL, Wisner TW, Lei H, Kazlauskas A, Johnson DC. 2012. PDGF receptor-
695 alpha does not promote HCMV entry into epithelial and endothelial cells but
696 increased quantities stimulate entry by an abnormal pathway. PLoS Pathog
697 8:e1002905.
698 22. Liu J, Jardetzky TS, Chin AL, Johnson DC, Vanarsdall AL. 2018. The human
699 cytomegalovirus trimer and pentamer promote sequential steps in entry into
700 epithelial and endothelial cells at cell surfaces and endosomes. J Virol
701 doi:10.1128/JVI.01336-18.
702 23. Siddiquey MNA, Zhang H, Nguyen CC, Domma AJ, Kamil JP. 2018. The Human
703 Cytomegalovirus Endoplasmic Reticulum-Resident Glycoprotein UL148 Activates
704 the Unfolded Protein Response. J Virol 92:e00896-18.
705 24. Zhang H, Read C, Nguyen CC, Siddiquey MNA, Shang C, Hall CM, von Einem J, Kamil
706 JP. 2019. A cytomegalovirus immunevasin triggers integrated stress response-
707 dependent reorganization of the endoplasmic reticulum. bioRxiv
708 doi:10.1101/641068:641068.
709 25. Cunningham BC, Wells JA. 1989. High-resolution epitope mapping of hGH-receptor
710 interactions by alanine-scanning mutagenesis. Science 244:1081-5.
711 26. Dao-pin S, Anderson DE, Baase WA, Dahlquist FW, Matthews BW. 1991. Structural
712 and thermodynamic consequences of burying a charged residue within the
713 hydrophobic core of T4 lysozyme. Biochemistry 30:11521-9.
714 27. Wertman KF, Drubin DG, Botstein D. 1992. Systematic mutational analysis of the
715 yeast ACT1 gene. Genetics 132:337-50.

716 28. Chothia C. 1976. The nature of the accessible and buried surfaces in proteins. J Mol
717 Biol 105:1-12.
718 29. Aroeti B, Kosen PA, Kuntz ID, Cohen FE, Mostov KE. 1993. Mutational and secondary
719 structural analysis of the basolateral sorting signal of the polymeric
720 immunoglobulin receptor. J Cell Biol 123:1149-60.
721 30. Graber P, Proudfoot AE, Talabot F, Bernard A, McKinnon M, Banks M, Fattah D,
722 Solari R, Peitsch MC, Wells TN. 1995. Identification of key charged residues of
723 human interleukin-5 in receptor binding and cellular activation. J Biol Chem
724 270:15762-9.
725 31. Banks M, Graber P, Proudfoot AE, Arod CY, Allet B, Bernard AR, Sebille E, McKinnon
726 M, Wells TN, Solari R. 1995. Soluble interleukin-5 receptor alpha-chain binding
727 assays: use for screening and analysis of interleukin-5 mutants. Anal Biochem
728 230:321-8.
729 32. Hebert CA, Vitangcol RV, Baker JB. 1991. Scanning mutagenesis of interleukin-8
730 identifies a cluster of residues required for receptor binding. J Biol Chem
731 266:18989-94.
732 33. Tischer BK, Smith GA, Osterrieder N. 2010. En passant mutagenesis: a two step
733 markerless red recombination system. Methods Mol Biol 634:421-30.
734 34. Tischer BK, von Einem J, Kaufer B, Osterrieder N. 2006. Two-step red-mediated
735 recombination for versatile high-efficiency markerless DNA manipulation in
736 Escherichia coli. Biotechniques 40:191-7.
737 35. Nishikawa SI, Fewell SW, Kato Y, Brodsky JL, Endo T. 2001. Molecular chaperones in
738 the yeast endoplasmic reticulum maintain the solubility of proteins for
739 retrotranslocation and degradation. J Cell Biol 153:1061-70.
740 36. Brodsky JL, Skach WR. 2011. Protein folding and quality control in the endoplasmic
741 reticulum: Recent lessons from yeast and mammalian cell systems. Curr Opin Cell
742 Biol 23:464-75.
743 37. Kaganovich D, Kopito R, Frydman J. 2008. Misfolded proteins partition between two
744 distinct quality control compartments. Nature 454:1088-95.
745 38. Codony-Servat J, Tapia MA, Bosch M, Oliva C, Domingo-Domenech J, Mellado B, Rolfe
746 M, Ross JS, Gascon P, Rovira A, Albanell J. 2006. Differential cellular and molecular
747 effects of bortezomib, a proteasome inhibitor, in human breast cancer cells.
748 Molecular Cancer Therapeutics 5:665-675.
749 39. Latonen L, Moore HM, Bai B, Jaamaa S, Laiho M. 2011. Proteasome inhibitors induce
750 nucleolar aggregation of proteasome target proteins and polyadenylated RNA by
751 altering ubiquitin availability. Oncogene 30:790-805.
752 40. Bence NF, Sampat RM, Kopito RR. 2001. Impairment of the ubiquitin-proteasome
753 system by protein aggregation. Science 292:1552-5.
754 41. Cox DW, Billingsley GD, Callahan JW. 1986. Aggregation of plasma Z type alpha 1-
755 antitrypsin suggests basic defect for the deficiency. FEBS Lett 205:255-60.
756 42. Lomas DA, Evans DL, Finch JT, Carrell RW. 1992. The mechanism of Z alpha 1-
757 antitrypsin accumulation in the liver. Nature 357:605-7.
758 43. Wang D, Li G, Schauflinger M, Nguyen CC, Hall ED, Yurochko AD, von Einem J, Kamil
759 JP. 2013. The ULb' region of the human cytomegalovirus genome confers an
760 increased requirement for the viral protein kinase UL97. J Virol 87:6359-76.

761 44. Sinzger C, Hahn G, Digel M, Katona R, Sampaio KL, Messerle M, Hengel H,
762 Koszinowski U, Brune W, Adler B. 2008. Cloning and sequencing of a highly
763 productive, endotheliotropic virus strain derived from human cytomegalovirus
764 TB40/E. J Gen Virol 89:359-68.
765 45. Li G, Rak M, Nguyen CC, Umashankar M, Goodrum FD, Kamil JP. 2014. An epistatic
766 relationship between the viral protein kinase UL97 and the UL133-UL138 latency
767 locus during the human cytomegalovirus lytic cycle. J Virol 88:6047-60.
768

769

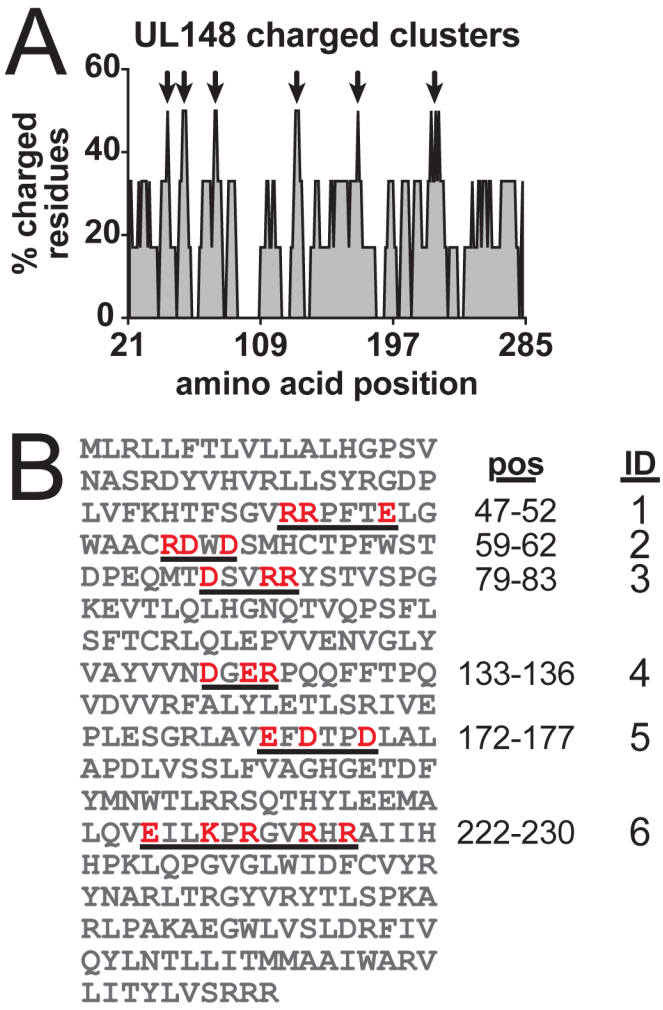


**FIGURE 1. Charged amino acid clusters within the predicted UL148 ectodomain**. (A) Percentage of charged residues (K, R, D, E) within the predicted UL148 ectodomain identified using an iterative scanning window six amino acid residues in size. Black arrows designate charged clusters (>40% charged residues). The last three local maxima in close proximity were treated as a single cluster. (B) UL148 protein sequence. Amino acid positions (pos) of the identified charged clusters are underlined. Residues in red were mutated to alanine in the six constructs indicated above using sequential numbering (ID), starting from the amino-terminus.

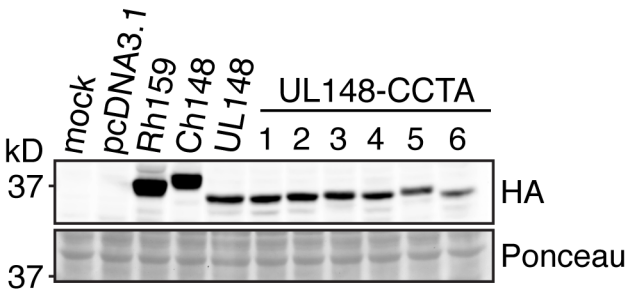


**FIGURE 2. Expression of HA-tagged UL148-CCTAs and UL148 homologs.** Human embryonic kidney 293T cells were transfected with expression plasmids encoding the indicated HA-tagged proteins. At 48 h post-transfection, cell lysates were analyzed by Western blot.

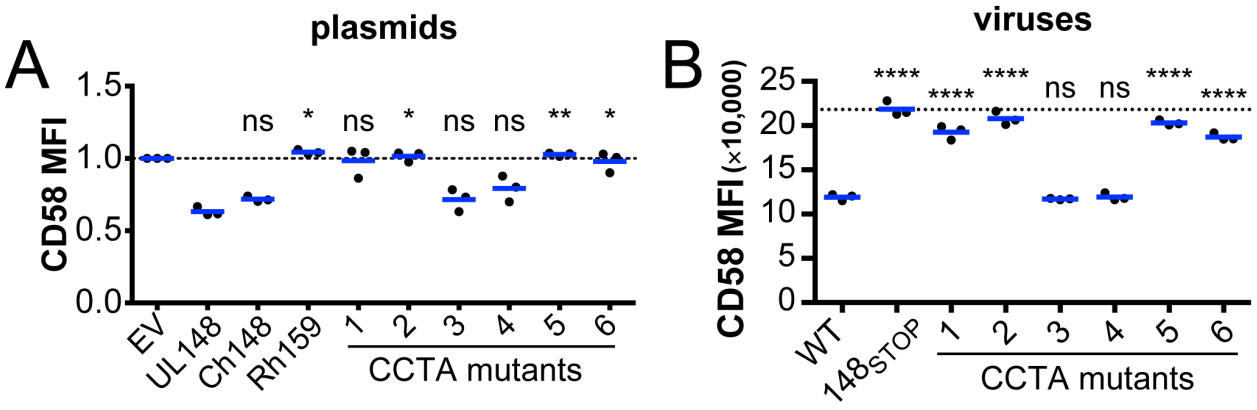


**FIGURE 3. Analysis of cell surface CD58 levels during expression of UL148 CCTA mutants and homologs from other primate CMVs.** (A) A549 cells were transfected with plasmids expressing the indicated protein or empty vector (EV). At 72 h post-transfection, cell surface CD58 levels were analyzed by flow cytometry. Median fluorescence intensity (MFI) values were normalized to the EV control. (B) Fibroblasts (HFFT) were infected at an MOI of 2 $TCID_{50}$ per cell with HCMV strain TB40/E derivatives wildtype for *UL148* (WT), carrying the indicated UL148 CCTA mutations, or *UL148*-null ($148_{STOP}$). At 72 h post-infection, cell surface CD58 was quantified by flow cytometry. (A-B) Data points indicate biological replicates from three independent experiments. P-values comparing the mean of each condition to wildtype UL148 (UL148, panel A) or wildtype virus (WT, panel B) were obtained by one-way analysis of variance (ANOVA) with Tukey's correction for multiple comparisons: ns, not significant; *, $p < 0.05$; **, $p < 0.01$; ****, $p < 0.0001$.

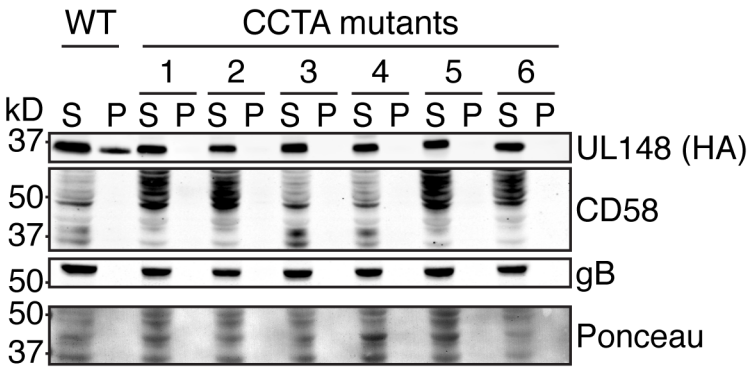


**FIGURE 4. The propensity of UL148 to accumulate in a detergent-insoluble form is not required to block CD58 maturation.** Fibroblasts (HFFT) were infected at an MOI of 1 $TCID_{50}$ per cell with HCMV or the indicated *UL148* mutant. At 72 h post-infection, cell lysates were separated by centrifugation into supernatant ("S") containing soluble proteins and pellet ("P") containing insoluble proteins. Supernatant and pellet fractions were analyzed by Western blot for UL148, CD58, and gB levels.

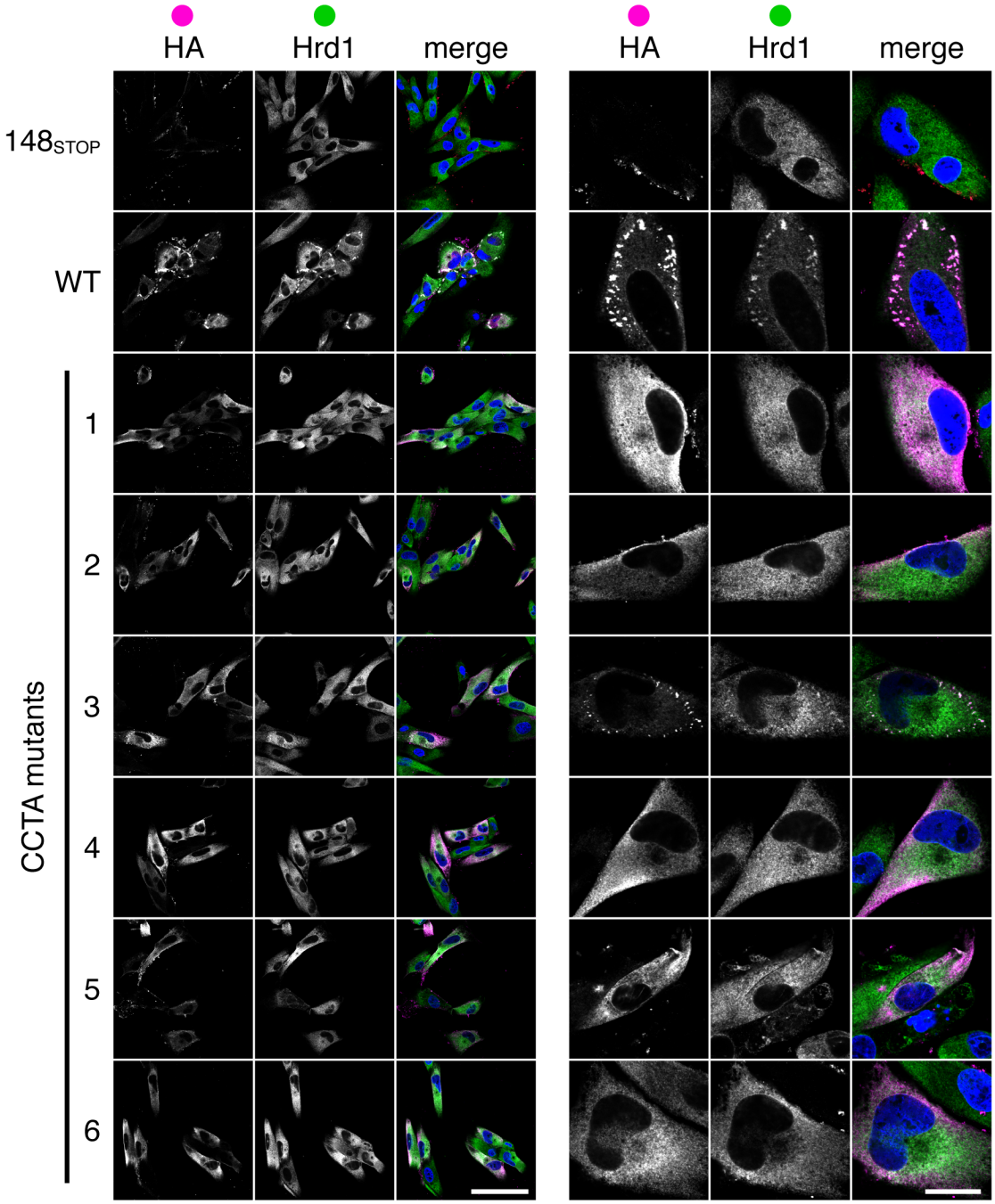


**FIGURE 5. Mutation of five UL148 charged clusters abolishes punctate co-localization of UL148 and ER marker Hrd1.** Fibroblasts (HFFT) were infected at an MOI of 1 $TCID_{50}$ per cell with HCMV strain TB40/E wildtype for *UL148*, harboring the indicated *UL148* CCTA mutant, or entirely null for *UL148* ($148_{STOP}$). At 72 h post-infection, cells were fixed and imaged by confocal microscopy after staining with antibodies specific for HA ($UL148^{HA}$, magenta) or ER marker Hrd1 (green). Nuclei were counterstained using Hoechst dye (blue).

822

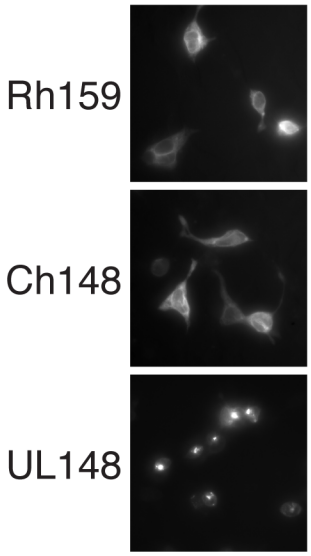


823

824 **FIGURE 6. Localization of UL148, Rh159, and Ch148.** Human embryonic kidney 293T
825 cells were transfected with doxycline-inducible vectors encoding the indicated protein
826 fused to a GFP tag. 100 ng/mL doxycycline was added to cells 1 h post-transfection. At
827 48 h post-transfection, GFP signal was visualized by immunofluorescence microscopy.
828
829
830
831
832
833
834

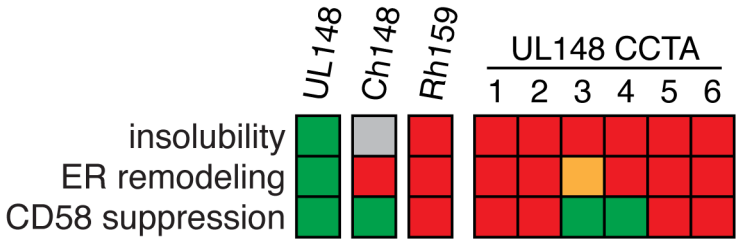


**FIGURE 7. Summary of activities of UL148-CCTAs and UL148 homologs.** Green squares indicate activity indistinguishable from wild-type HCMV UL148. Red squares indicate total absence of the activity. Yellow squares indicate a partial phenotype. Gray square, not tested.

**Table 1. Synthetic DNAs used in this study.**

| Name | Sequence (5' to 3') |
|---|---|
| IsceKan_FWD | TAGGGATAACAGGGTAATCGATTT |
| IsceKan_REV | GCCAGTGTTACAACCAATTAACC |
| SP6_FWD | ATTTAGGTGACACTATAG |
| T7 seq FWD | TAATACGACTCACTATAGGG |
| TB_Rh159HA_seq_FWD | AGTGTTTATGAGTCGGGCGG |
| TB_Rh159HA_seq_REV | GTGGCGACGTGGATTTCTTG |
| Fwd_Ch148_OUPgibs | TTCCTACCCTCGTAAACCGGTGAATTCGCCACCATGCCCCGCTTCTGGTTAATGTGCTT |
| Rev_Ch148_GFPgibs | AGTAAAAAGCTCCTCCCCCTTGCTCACCATCCGGGGCGACGACATCCAC |
| Fwd_GFP_Ch148gibs | ATGGTGAGCAAGGGGGAGGAGC |
| Rev_GFP_allUL148 | AACCCGGCGCGGAGGC |
| CMVcrsnull_Fw | TCAGGTAGTGAACCGTCAG |
| Ubc_Rv | TGATACTGGGGTTCTAAGGC |
| Ch148_3pr_Fw | TGGACTTCTCCGTCTATCG |
| pSP72_148_RRPFTE_FWD | TCGGGTGTGGCCGCTCCTTTCACTGCGCTAGGCTGGGC |
| pSP72_148_RRPFTE_REV | GCCCAGCCTAGCGCAGTGAAAGGAGCGGCCACACCCGA |
| pSP72_148_RDWD_FWD | TGGGCTGCGTGTGCAGCTTGGGCGAGTATGCATTG |
| pSP72_148_RDWD_REV | CAATGCATACTCGCCCAAGCTGCACACGCAGCCCA |
| pSP72_148_DSVRR_FWD | GAGCAGATGACCGCCAGCGTAGCTGCTTACAGCACAGTG |
| pSP72_148_DSVRR_REV | CACTGTGCTGTAAGCAGCTACGCTGGCGGTCATCTGCTC |
| pSP72_148_DGER_FWD | TACGTGGTCAACGCGGGAGCTGCGCCGCAGCAGT |
| pSP72_148_DGER_REV | ACTGCTGCGGCGCAGCTCCCGCGTTGACCACGTA |
| pSP72_148_EFDTPD_FWD | CGCCTGGCAGTGGCGTTCGCTACTCCGGCGCTAGCTCTGGCG |
| pSP72_148_EFDTPD_REV | CGCCAGAGCTAGCGCCGGAGTAGCGAACGCCACTGCCAGGCG |
| pSP72_148_EILKPRGVRHR_FWD | GCCTTACAGGTGGCTATACTCGCACCAGCCGGGGTCGCCCACGCGGCTATTATCCAC |
| pSP72_148_EILKPRGVRHR_REV | GTGGATAATAGCCGCGTGGGCGACCCCGGCTGGTGCGAGTATAGCCACCTGTAAGGC |
| TB_148RRPFTE_Fw | AGGCGACCCCCTGGTCTTCAAGCACACTTTTTCGGGTGTGGCCGCTCCTTTCACTGCGCTAGGCTGGGCTAGGGATAACAGGGTAATCGATTT |
| TB_148RDWD_Fw | TGTGCGTCGACCCTTCACCGAGCTAGGCTGGGCTGCGTGTGCAGCTTGGGCGAGTATGCATTGCACTAGGGATAACAGGGTAATCGATTT |
| TB_148DSVRR_Fw | TGCACGCCCTTCTGGTCTACCGATCCGGAGCAGATGACCGCCAGCGTAGCTGCTTACAGCACAGTGATAGGGATAACAGGGTAATCGATTT |
| TB_148DGER_Fw | GTGGAAAATGTTGGCCTCTACGTGGCCTACGTGGTCAACGCGGGAGCTGCGCCACAGCAGTTTTTTTAGGGATAACAGGGTAATCGATTT |
| TB_148EFDTPD_Fw | CGGATCGTGGAACCGTTAGAATCAGGTCGCCTGGCAGTGGCGTTCGCTACTCCGGCGCTAGCTCTGGCGTAGGGATAACAGGGTAATCGATTT |
| TB_148EILK_Fw | AGTCAGACCCACTACCTGGAGGAGATGGCCTTACAGGTGGCTATACTCGCACCAGCCGGGGTCGCCCACGCGGCTATAGGGATAACAGGGTAATCGATTT |
| TB_148RRPFTE_Rv | ATGCATACTGTCCCAGTCGCGACACGCAGCCCAGCCTAGCGCAGTGAAAGGAGCGGCCACACCCGAAAGCCAGTGTTACAACCAATTAACC |
| TB_148RDWD_Rv | GCTCCGGATCGGTAGACCAGAAGGGCGTGCAATGCATACTCGCCCAAGCTGCACACGCAGCCCAGCGCCAGTGTTACAACCAATTAACC |
| TB_148DSVRR_Rv | CTGAAGCGTCACTTCCTTGCCGGGGCTCACTGTGCTGTAAGCAGCTACGCTGGCGGTCATCTGCTCGCCAGTGTTACAACCAATTAACC |
| TB_148DGER_Rv | AGCGTACCACGTCTACCTGCGGTGTAAAAAACTGCTGTGGCGCAGCTCCCGCGTTGACCACGTAGGCCAGTGTTACAACCAATTAACC |
| TB_148EFDTPD_Rv | CCACGAAGAGGCTGCTTACTAAATCGGGCGCCAGAGCTAGCGCCGGAGTAGCGAACGCCACTGCCAGGGCCAGTGTTACAACCAATTAACC |
| TB_148EILK_Rv | GGCCAACGCCCGGCTGTAGCTTCGGATGGTGGATAATAGCCGCGTGGGCGACCCCGGCTGGTGCGAGTATAGCCACGCCAGTGTTACAACCAATTAACC |
| UL148_reclone_FWD | CTTTGGATCCACCATGTTGCGCTTGCTGTTCACGCTCGTCC |
| UL148_reclone_REV | GTTTGAATTCACTAGGCGTAGTCTGGGACGTCGTATGGGTACCGACGCCGCGACACCAGGTAGGTTATC |
| TB_UL74_Cterm_seq_FWD | ACACGCACGTACTGATTCGT |
| TB_UL74_Cterm_seq_REV | CCCAACGTGATGAGACCACA |
| ChCMV_UL148_FRAG | CGTTTAAACTTAAGCTTGGTACCGAGCTCGGATCCACCATGCCCCGCTTCTGGtTAATGTGCTTCCTGTTGACTTCCCTCAGCGAGCATGTCTTTAGGGCGCAtGGtAGCCAGCTC |

| | |
|---|---|
| | CTCAACTAtGTACAGGTtCGACTACTGAGCGGTCGCGGCGGCCCGCTAGTCTTCGCG<br>CACACCTTtTCCTCCGTACCCTGGTCCTTCACCGAGCTGGGATGGGCtGTCTGtGCCG<br>ACTGGGACAGCATGAAATGCACACCTTTCTGGACCAGCAACCTGACATCTTCCTGGT<br>CACCTCCGTCGGACACGGTCTGGCGCTACAGGCTGTCCGATCCGGGCGCGACAATC<br>ACGCTGCAGCTACAGAACCAGACGGCaCCCTGGCCCGCGGGtGGCCTGAGCTTCTC<br>TTCCCGGCTGCAGCTGGACGCCGTGATCGAAAACGCCGGTCTCTACGTGGCCTACG<br>TGGTCAACGACGGCGATCGGCCATCGCAGTTCCTGGAGCCCCGGGTGGACTTCGTG<br>CGCTTCGCCCTCTATCTGGAGACGGAGACCCAGATCCTGGAGAACCTGGACTCGGG<br>TCGCCTGGTGGCGCAATTCGACACGCCGGATCTGGCCTTCGGGCCGGACCTGGTGA<br>GCAGCTTCGTGATCAGCGGTAACGGCGAGCGCGACTACCACCTTAACTGGACGGTG<br>CGACGCAGTGAGACCTACCGGTACGACAACATACAGCTGCAGGTGGAGATCCAGGA<br>GCCCCGCGGACTACGGCACCGCGCCACCATCGAGCGGCCGCAGTACAAGGTGGGC<br>TCCCACCTCTCGCTGGACTTCTCCGTCTATCGCCACAACGCCCGCCTGACCCGCGG<br>CTACGTGCAATACACGTTTCCCAAAGAGGCCTTCGAACGGGCCAAGAGACTGCGCG<br>AGGACCCAAAAGCCGCCGGATGGCTGGCGACCATCGACAGATTCGTCGTGCAGTAT<br>CTGAATGCGCTGCTGATAACGGTGATGGGCATCTTGTGGGTTCGCGTTTTGGTAACC<br>TGGTGGATGTCGTCGCCCCGGTACCCATACGACGTCCCAGACTACGCCTAGtGAATT<br>CTGCAGATATCCAGCACAGTGGCGGCCGCT |